


QUANTIFYING RESILIENCE AND THE RISK OF REGIME SHIFTS UNDER STRONG CORRELATED NOISE

arXiv PREPRINT

 **Martin Heßler***

Institute for Theoretical Physics
Westphalian Wilhelms-University Münster
48149 Münster, North Rhine-Westphalia, Germany
m_hess23@uni-muenster.de

 **Oliver Kamps**

Center for Nonlinear Science
Westphalian Wilhelms-University Münster
48149 Münster, North Rhine-Westphalia, Germany
okamp@uni-muenster.de

November 8, 2022

ABSTRACT

Early warning indicators often suffer from the shortness and coarse-graining of real-world time series. Furthermore, the typically strong and correlated noise contributions in real applications are severe drawbacks for statistical measures. Even under favourable simulation conditions the measures are of limited capacity due to their qualitative nature and sometimes ambiguous trend-to-noise ratio. In order to solve these shortcomings, we analyse the stability of the system via the slope of the deterministic term of a Langevin equation, which is hypothesized to underlie the system dynamics close to the fixed point. The open-source available method is applied to a previously studied seasonal ecological model under noise levels and correlation scenarios commonly observed in real world data. We compare the results to autocorrelation, standard deviation, skewness and kurtosis as leading indicator candidates by a Bayesian model comparison with a linear and a constant model. We show that the slope of the deterministic term is a promising alternative due to its quantitative nature and high robustness against noise levels and types. The commonly computed indicators apart from the autocorrelation with deseasonalization fail to provide reliable insights into the stability of the system in contrast to a previously performed study in which the standard deviation was found to perform best. In addition, we discuss the significant influence of the seasonal nature of the data to the robust computation of the various indicators, before we determine approximately the minimal amount of data per time window that leads to significant trends for the drift slope estimations.

Keywords ecology · regime shift · early warning signals · leading indicator · critical transition

1 Introduction

Even if the idea of universal early warning indicators (Dakos et al. [2012, 2009], Scheffer et al. [2015], Liang et al. [2017]) for critical transitions is a fascinating and attractive vision throughout the fields of ecology, climate research, biology, power grids (Veraart et al. [2011], Drake and Griffen [2010], Dakos et al. [2017], Livina et al. [2010, 2015], Lenton [2012], Cotilla-Sanchez et al. [2012]), its potential for social and economical sciences (Jusup et al. [2022], Helbing et al. [2014]) and much more (Izrailtyan et al. [2000], Chadeffaux [2014], van de Leemput et al. [2013]), the research done over the years in this field has discovered plenty of problems, drawbacks and limitations of the proposed leading indicators (Clements et al. [2015], Hastings and Wysham [2010], Ditlevsen and Johnsen [2010], Wilkat et al. [2019]). The difficulties and limitations result from the sometimes mentioned problematic claim of “universality” which is hard or impossible to achieve. Just by definition the mentioned universality is already limited to special cases of regime shifts as bifurcation-induced tipping events (Scheffer et al. [2009], Ritchie and Sieber [2017], Ashwin et al. [2012]), because the leading indicators are a consequence of the commonly observed phenomenon of *critical slowing down* prior to a bifurcation or *flickering* in noisy bistable systems (Scheffer et al. [2012], Wissel [1984], Schröder et al.

*Center for Nonlinear Science, Westphalian Wilhelms-University Münster, 48149 Münster, Germany

[2005]). Critical slowing down is the increased relaxation time of perturbations near a bifurcation whereas flickering determines jumps of a system between two alternative stable states. Furthermore, a successful detection of a critical transition depends on the eigen-direction in which the transition takes place and the time series at hand (Boerlijst et al. [2013]). Apart from that it remains difficult to get an impression of the leading indicators' quality applied to real world systems because the tests are often performed with historical test data for which is known that a transition is present (Boettiger and Hastings [2012]).

Following this argumentation it is proposed to design specialised indicators in specific fields of research or systems that are known at least in part (Perretti and Munch [2012], Gsell et al. [2016], Dablander et al. [2020]). One of those research areas is the field of ecology in which standard leading indicators as autocorrelation at a lag of one (AR1), the standard deviation (std) $\hat{\sigma}$, the skewness γ or the kurtosis ω are often very limited in their applicability due to high correlated noise contributions and low sampled short time series that are characteristic because of the limits imposed by the experimental and funding resources as stated in Bissonette [1999], Perretti and Munch [2012]. However, due to the rapid developments in sensor and information processing techniques at least the sampling limitations might be partially overcome in future ecological studies e.g. due to deep-learning image recognition techniques of animal-tracking camera or satellite data (Francisco et al. [2020], Duporge et al. [2020], Zhao et al. [2020]) or acoustic telemetry systems (Aspillaga et al. [2021]). Furthermore, even in simulations in which the afore-mentioned practical limitations do not play a role, the inherent design of the indicators raises problems. As discussed in Biggs et al. [2009] the standard leading indicator candidates are difficult to interpret because of their qualitative nature: They are designed upon trend changes which can be too gradual and ambiguous to rely on for decision-makers. And in addition, unfortunately these changes are often realized too late for policymakers to adapt management and avoid uprising transitions. Therefore, in the case that a developed early warning measure should be applicable in practise the authors of Biggs et al. [2009] claim that it

would rely on: (i) defining critical levels of the regime shift indicators, (ii) linking these critical levels to long-term sustainable impact levels, and (iii) finding or developing indicators that have critical levels that are relatively transferable across different ecosystem types.

Based on these demands (Biggs et al. [2009]) and the poor performance of standard leading indicator candidates under strong correlated noise found in Perretti and Munch [2012], we want to introduce the alternative drift slope estimation Heßler and Kamps [2021], Heßler [2021a,b] to tackle the problem of anticipating an ecological regime shift and compare it to the above mentioned indicators. Similar to Carpenter and Brock [2011] the alternative approach considers the data to be generated by a stochastic differential equation of the Langevin form (Kloeden and Platen [1992])

$$\dot{x}(x, t) = h(x(t), t) + g(x(t), t)\Gamma(t), \quad (1)$$

where the drift $h(x(t), t)$ captures the deterministic part of the system dynamics under the stochastic influence of a Gaussian and δ -correlated noise process $\Gamma(t)$ that scales with the diffusion $g(x(t), t)$. The method estimates the parameterized drift and diffusion terms via Markov Chain Monte Carlo sampling (MCMC) and calculates the drift slope ζ in the fixed point x^* in rolling windows as a resilience measure of the system. The drift slope ζ is negative for stable systems and increases with proceeding destabilization. A zero crossing of the drift slope corresponds to a regime shift (Heßler and Kamps [2021]). In principle, drift and diffusion can also be directly estimated via the Kramers-Moyal expansion (Friedrich and Peinke [1997], Friedrich et al. [2000]). Nevertheless, this direct drift estimation does not result in stable estimates under the noise conditions of the investigated ecological model (cf. supplementary material (Heßler [2022])). For that reason, we have chosen a fully Bayesian approach, extending the maximum likelihood formulation in Kleinhans [2011], since it allows for a significantly more stable estimation of the slope, includes a straight-forward calculation of credibility bands without approximation by Wilks' theorem and accounts for possibly multi-peaked probability densities.

In this study we show that in contrast to the common qualitative leading indicator candidates, the method provides a quantitative and easy-to-interpret resilience measure which is able to fulfill the requirements stated in Biggs et al. [2009] for the system discussed there under noise conditions typical for ecological experimental time series data, i.e. correlated strong noise influence (Perretti and Munch [2012]). In addition, we discuss the important role of the seasonal nature of the data that affects the trend quality of the time series analysis methods. The performance of the early warning signals is tested by comparing the probability that the data might be explained by a linear trend or a constant model with a Bayesian model comparison. The drift slope ζ and - if the seasonality is taken into account - the AR1 provide reliable results in our study. Interestingly, in contrast to previous results regarding the same system (Perretti and Munch [2012]) the AR1 seems to be preferred to the insignificant standard deviation. In this context it is important to mention that the AR1 would be only considered a reliable indicator if both the AR1 and std $\hat{\sigma}$ would increase at the same time. Apart from this we can reproduce the findings of a generally poor performance of the standard leading indicator candidates (Perretti and Munch [2012]). In the end, the drift slope seems to be a promising alternative to common leading indicators because of its quantitative nature, easy interpretation and robustness to strong and colored noise contributions. However, its applicability remains limited to situations in which it is possible to generate the

necessary amount of data which is around 50 data points per year for the investigated ecological model. The ecological system is presented in section 2. In section 3 we introduce the Bayesian Langevin estimation scheme as well as the methods to estimate the statistical leading indicators in the subsections 3.1 and 3.2, before we summarize the significance test approach via Bayes factors in subsection 3.3. The results of the applied leading indicators are discussed in section 4 which is divided into three parts: First, the drift slope results are presented in subsection 4.1. Second, the drift slope performance as leading indicator is compared to established candidates via a Bayesian model comparison in subsection 4.2, before the needed minimum amount of data per window for the drift slope estimation for the model at hand is defined in subsection 4.3. Finally, we summarize our findings in section 5.

2 Ecological model

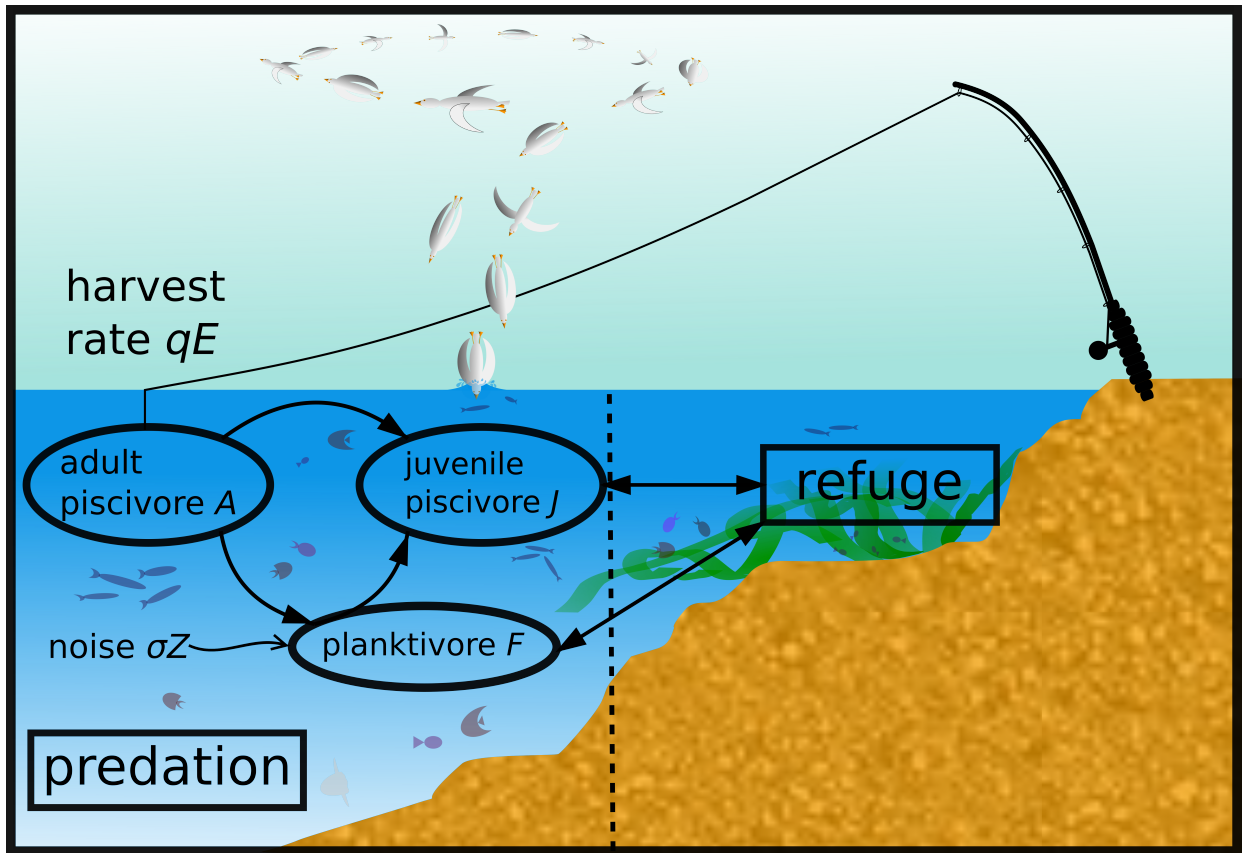


Figure 1: A scheme of the considered foodweb model. In the predation area the adult piscivores A hunt the juvenile piscivores J and the planktivores F which only hunt juvenile piscivores J . Both, the juvenile piscivores J and the planktivores F can hide themselves in a refuge area in order to retire. External white or colored stochastic influence Z is added to the planktivore population with the noise level σ . We discuss the possibility of regime shifts due to high angling pressure represented by the harvest rate qE which is given as the product of catchability q and the effort E . Here, the model is restricted to fish, but in general other animals, as e.g. some seabirds, are included in the term “piscivores”.

In order to investigate the performance of the Bayesian stability analysis tool under rather realistic conditions in the field of ecology the multi-species model derived in Carpenter and Brock [2004], described in detail in Biggs et al. [2009] and used as a basis of leading indicator performance tests in Perretti and Munch [2012] is simulated via the Euler-Maruyama scheme. The ecological system consists of three parties: juvenile piscivores (J), adult piscivores (A)

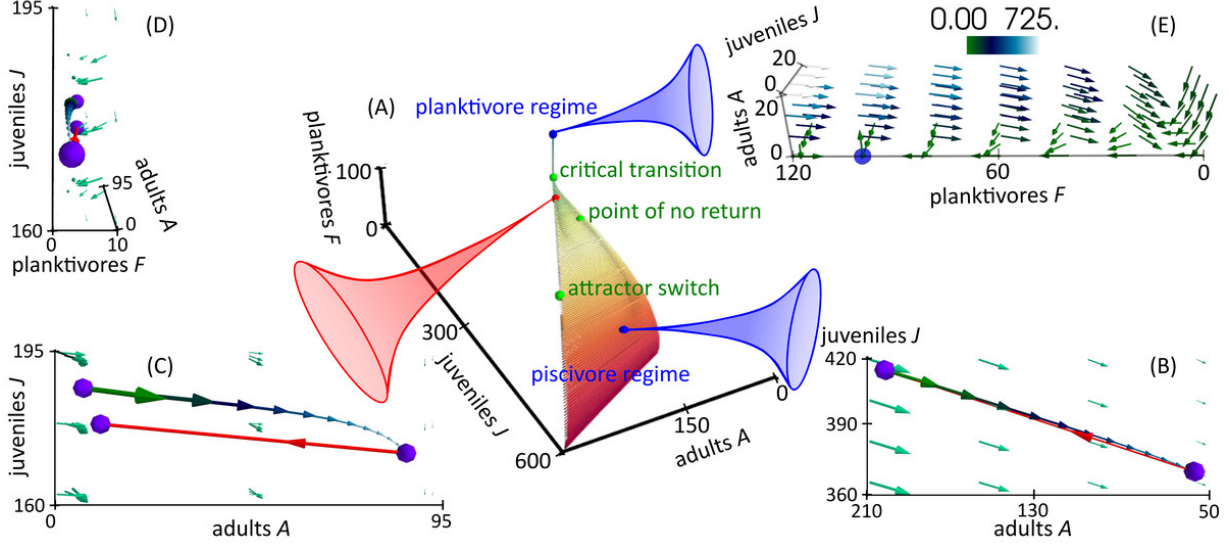


Figure 2: The destabilizing journey from the piscivore regime to the planktivore regime is shown in (A) with time color-coded from red to blue. The harvest rate qE is increased linearly to obtain the trajectory. The system starts in the stable piscivore-dominated regime. One realisation is exemplarily shown in (B) for harvest rate $qE = 1.38$. Only a tiny amount of planktivores $0 < F < 1$ is present and therefore the dynamics are reduced to the A - J plane. Juveniles J and adults A of the piscivore species decrease over one year (vector line with time color-coded from green to blue with start and end points given by the violet markers) before the population is updated by the species-intrinsic reproduction rate at the beginning of the new year mirrored by the discrete maturation map (red vector line). The overall surrounding flow is shown as a green vector field with vector lengths reflecting the flow strength. These periodic dynamics are stable until the harvest rate reaches the attractor switch point $qE_{\text{switch}} \approx 1.78$. For $qE > qE_{\text{switch}}$ the periodic cycle opens up as observable in (C) for an exemplary harvest rate $qE = 2.42$. The discrete maturation step cannot compensate the loss of the piscivore population completely anymore as visible by comparison of the start and end positions marked by violet points of the one-year dynamics which leads to always stronger reduction of the piscivore population over the years. At the same time the planktivore population starts to increase slightly as observable in figure (D) for the same qE . The figure is aligned to the planktivore F -axis. The green signed critical transition in (A) is subjectively defined for the planktivores $F > 21$ for the first time which coincides with the region after which the planktivore species grows drastically. The point of no return around $qE \approx 2.23$ is defined inside of the transition interval between the attractor switch point and the transition point as the point after which even an abrupt reduction of the angling pressure to $qE < 0.1$ cannot avoid the transition to the planktivore-dominated state anymore. At last the new stable state is illustrated in three dimensions in figure (E). The blue point marks the stable planktivore regime with $F \approx 100$, whereas the piscivores are extinct. The flow field strength is color-coded for better resolution.

and planktivores (F). The model contains a continuous “monitoring interval”

$$\frac{dA}{dt} = -qEA \quad (2)$$

$$\frac{dF}{dt} = D_F(F_R - F) - c_{FA}FA + \sigma Z \quad (3)$$

$$\frac{dJ}{dt} = -c_{JA}JA - \frac{c_{JF}FJ}{h + \nu + c_{JF}F} \quad (4)$$

and a discrete annual “maturation interval” realized as the map equations

$$A_{y+1} = s(A_{y;t=1} + J_{y;t=1}) \quad (5)$$

$$F_{y+1} = F_y \quad (6)$$

$$J_{y+1} = fA_{y+1}, \quad (7)$$

where the index $y; t = 1$ means the abundance of each party at the end of the monitoring interval (i.e. $t = 1$) of the corresponding year y . In the map s determines the survivorship between maturation intervals and f the fecundity rate of the adult piscivores A . The harvest rate of the adult piscivores is determined via the product of the catchability q and

Table 1: The parameter values of the ecological model with short definitions.

parameter	value	short definition
qE_{init}	1	initial harvest rate
$\Delta(qE)$	0.013	change of harvest rate per year
F_R	100	refuge reservoir for planktivores
D_F	0.1	foraging arena
c_{FA}	0.3	rate at which adult piscivores consume planktivores
c_{JA}	0.001	control of juvenile piscivores by adult piscivores
c_{JF}	0.5	rate at which planktivores consume juvenile piscivores
ν	1	rate at which juvenile piscivores become vulnerable against planktivores
h	8	rate at which juvenile planktivores enter the refuge
f	2	fecundity rate of adult piscivores
s	0.5	survival rate of adult and juvenile piscivores over the winter period

the effort E . The planktivores exchange between a protected area, the so-called refuge reservoir F_R and the foraging arena D_F . The parameters $c_{i,j}$ with $i, j = \{A, F, J\}$ model the consumption or control rates of i by j . Besides, the piscivores become vulnerable to planktivores with the rate ν and enter their refuge with h . Environmental stochasticity of the lower level of the food web is incorporated via Z . White noise Z_{white} corresponds simply to a Wiener process $Z_{\text{white}} = dW$ with spectral power $P_{\text{white}} \approx 7.5$. Pink noise Z_{pink} is obtained by the following procedure:

- (i) Fourier transform $(\mathcal{F}\xi)(f)$ of a white noise signal $\xi(t)$ with f denoting the frequencies,
- (ii) adjusting the obtained power spectrum by a power law $\sim e^{-\beta_{\text{pink}}}$ with $\beta_{\text{pink}} = 0.8$ (cf. Perretti and Munch [2012] for comparability),
- (iii) and finally an inverse Fourier transform $(\mathcal{F}^{-1}(\mathcal{F}\xi'))(t)$ of the adjusted power spectrum $(\mathcal{F}\xi')(f)$. The pink noise data is thus $Z_{\text{pink}} = (\mathcal{F}^{-1}(\mathcal{F}\xi'))(t)$.

To keep close to the former studies of Perretti and Munch [2012] the red noise signal Z_{red} is computed via the Ornstein-Uhlenbeck process

$$dZ_{\text{red}} = -\phi Z_{\text{red}} dt + \sqrt{2\phi} dW \quad (8)$$

with $\phi = 0.53$ which results in a spectral exponent $\beta_{\text{red}} \approx 1.6$ (cf. Perretti and Munch [2012] for comparability). The total powers P of the correlated signals are adjusted to be approximately equal $P_{\text{pink}} \approx P_{\text{red}} \approx 15.4$. For each of the three noise types the model is evaluated for three different noise intensities, explicitly

$$\sigma dt = 0.002 \quad (9)$$

$$\sigma dt = 0.044 \quad (10)$$

$$\sigma dt = 0.09 \quad (11)$$

with a time step of $dt = 1/50$. The realisations of the model are computed with the parameters explicitly listed in table 1 and chosen analogously to Perretti and Munch [2012] apart from the initial harvest rate qE_{init} that is chosen to be $qE_{\text{init}} = 1$ instead of $qE_{\text{init}} = 1.5$ in order to widen the temporal resolution of the stable regime. The parameter choice in Perretti and Munch [2012] follows approximately experimentally observed values in ecological systems of that kind, especially for the noise strength (Reed and Hobbs [2004]), the noise power law exponents (Steele [1985], Vasseur and Yodzis [2004]) and the increase in angling pressure (Pope [1996]). Note that as stated in table 1, the rate of linear destabilization $\Delta(qE)$ as all the other parameters is chosen analogously to Perretti and Munch [2012] and thus, the choice $qE_{\text{init}} = 1$ does not affect the comparability. Depending on the harvest rate the system settles into a piscivore- or planktivore-dominated state. In the first mentioned scenario the planktivore abundance is kept at a low level because of a large occurrence of adult piscivores whereas in the second scenario the large population of planktivores hinders the piscivore population to grow because the planktivores' predation of the juvenile group.

We focus on regime shifts from the piscivore- into the planktivore-dominated state due to increasing harvest rate or angling pressure qE . In figure 2 the key features of the dynamics are illustrated in state space for a more detailed mathematical description.

3 Numerical methods

In subsection 3.1 and 3.2 we introduce the Bayesian drift slope estimation procedure as well as the methods used to estimate the statistical measures. Finally, in subsection 3.3 we describe our approach of trend-significance testing via Bayes factors.

3.1 Drift slope estimation scheme

Starting with the Langevin equation 1 we parameterize the drift and diffusion as $h(x(t), t) \equiv h(x(t))$ and $g(x(t), t) \equiv \text{const.} =: \sigma$. Since we assume to be in a fixed point and close to a bifurcation we develop $h(x, t)$ into a Taylor series up to order three which is sufficient to describe the normal forms of simple bifurcation scenarios (Strogatz [2015]). This results in

$$h(x(t), t) = \alpha_0(t) + \alpha_1(t)(x - x^*) + \alpha_2(t)(x - x^*)^2 + \alpha_3(t)(x - x^*)^3 + \mathcal{O}((x - x^*)^4), \quad (12)$$

so that the information on the linear stability is incorporated in α_1 . For practical reasons equation 12 is used in the form

$$h_{\text{MC}}(x(t), t) = \theta_0(t; x^*) + \theta_1(t; x^*) \cdot x + \theta_2(t; x^*) \cdot x^2 + \theta_3(t; x^*) \cdot x^3 + \mathcal{O}(x^4) \quad (13)$$

in the numerical approach, where an arbitrary fixed point x^* is incorporated in the coefficients $\underline{\theta}$ by algebraic transformation and comparison of coefficients. A change of the negative sign of the slope

$$\zeta = \left. \frac{dh(x)}{dx} \right|_{x=x^*} \quad (14)$$

of the nonlinear drift at the fixed point x^* which is estimated to be the data mean corresponds to a loss of stability via the formalism of linear stability analysis (Heßler and Kamps [2021]).

The task is now to estimate the parameters $\underline{\theta}$. Their posterior distribution is given by applying Bayes' theorem

$$p(\underline{\theta}, \sigma | \underline{d}, \mathcal{I}) = \frac{p(\underline{d} | \underline{\theta}, \sigma, \mathcal{I}) \cdot p(\underline{\theta}, \sigma | \mathcal{I})}{p(\underline{d} | \mathcal{I})}. \quad (15)$$

The likelihood $p(\underline{d} | \underline{\theta}, \sigma, \mathcal{I})$ is given as the transition probability of the process defined by equation (1) (see Heßler and Kamps [2021]) and the prior knowledge is incorporated in $p(\underline{\theta}, \sigma | \mathcal{I})$. The evidence $p(\underline{d} | \mathcal{I})$ normalizes the posterior probability density function (pdf) $p(\underline{\theta}, \sigma | \underline{d}, \mathcal{I})$. One advantage of this procedure is the consistent definition of credibility bands of the estimated parameters based on the posterior pdf. The posterior distribution of the parameters can be estimated via MCMC sampling with the flat Jeffreys' priors

$$p_{\text{prior}}(\theta_0, \theta_1) = \frac{1}{2\pi(1 + \theta_1^2)^{\frac{3}{2}}} \quad (16)$$

and

$$p_{\text{prior}}(\sigma) = \frac{1}{\sigma} \quad (17)$$

for the scale variable σ (von der Linden et al. [2014]). Gaussian priors

$$\begin{aligned} p_{\text{prior}}(\theta_2) &= \mathcal{N}(\mu, \sigma_{\theta_2}), \\ p_{\text{prior}}(\theta_3) &= \mathcal{N}(\mu, \sigma_{\theta_3}) \end{aligned} \quad (18)$$

centred around the mean $\mu = 0$ with standard deviations σ_{θ_i} in an adequate range are used for the rest of the parameters. The flat Jeffreys' priors are chosen broadly as $[-50, 50]$ for $\theta_{0,1}$ and $[0, 50]$ for θ_4 except for the analysis of the deseasonalized versions of the correlated models. In these cases (red lines in D-I) the prior range is chosen even broader as $[-70, 70]$ for $\theta_{0,1}$ and $[0, 70]$ for θ_4 to make sure that the available data determines the posterior distribution. The Gaussian priors for $\theta_{2,3}$ are implemented with $\sigma = \{4, 8\}$, respectively.

We use the MCMC sampling algorithm implemented in the python package *emcee* (Foreman-Mackey et al. [2013]). The method is applied in rolling windows in order to resolve the time evolution of the drift slope. A detailed description of the presented algorithm and its implementation steps can be found in Heßler and Kamps [2021].

3.2 Statistical leading indicators

The biased autocorrelation at lag-1 is computed via *statsmodels.tsa.stattools.acf* (Seabold and Perktold [2010]) and the biased standard deviation $\hat{\sigma}$ via *numpy.std* (Harris et al. [2020]). The skewness γ and kurtosis ω calculations are performed with the biased uncorrected estimators of the python package *scipy.stats* (Virtanen et al. [2020]). The biased versions are used, because of the large sample sizes which provide sufficient accuracy. The skewness definition follows the not-adjusted Fisher-Pearson estimator and the kurtosis is defined via the Pearson estimator corresponding to a kurtosis $\omega = 3$ for a Gaussian distribution.

3.3 Significance testing via Bayesian model comparison

A Bayesian model comparison is used in order to quantify the significance of the various leading indicators. Shortly summarized, we compare the probability that the estimated leading indicators can be explained by a linear trend model to the probability that the measures are described by a constant model via the concept of Bayes factors (Jeffreys [1998]). The Bayes factors

$$BF_{ij} = \frac{p(\underline{\mathcal{I}}|\mathcal{M}_i)}{p(\underline{\mathcal{I}}|\mathcal{M}_j)} \text{ with } i, j \in \{1, 2\} \text{ and } i \neq j \quad (19)$$

are computed in the same way for the different leading indicator candidates. The prior parameter ranges of the linear model \mathcal{M}_1 and the constant model \mathcal{M}_2 are adapted to the specific leading indicator time series data based on the following procedure:

- (i) The initial value \mathcal{I}_0 of each leading indicator time series is used as mean $\mu_{\mathcal{M}_2}$ of a Gaussian distribution $\mathcal{N}(\mu_{\mathcal{M}_2} = \mathcal{I}_0, \sigma_{\mathcal{M}_2} = 1)$. The distribution is used to draw the parameter of the constant model \mathcal{M}_2 which are also used as the intercepts b of the linear model $\mathcal{M}_1 : y = a \cdot x + b$.
- (ii) The slope a of the linear model \mathcal{M}_1 is drawn from a uniform distribution in the range $[0, 1.5 \cdot \frac{\max(\underline{\mathcal{I}}) - \min(\underline{\mathcal{I}})}{t_{\text{end}} - t_{\text{start}}}]$. The calculations of BFs in the case of decreasing skewness is performed by drawing uniformly from the interval $[-1.5 \cdot \frac{\max(\underline{\mathcal{I}}) - \min(\underline{\mathcal{I}})}{t_{\text{end}} - t_{\text{start}}}, 0]$.
- (iii) The logarithmic noise is drawn uniformly from the interval $[\log(0.5), \log(5)]$.

The convergence of the results is guaranteed by drawing 10^7 realisations of each model in each BF calculation.

4 Results

4.1 Drift slope analysis

The drift slope estimation method that is shortly summarized in section 3 and described in detail in Heßler and Kamps [2021] is applied to time series simulations of the seasonal ecological model with white, pink and red noise each of which is realised for three noise levels $\sigma = \{0.1, 2.2, 4.5\}$. The data is evaluated in windows of 750 data points that are shifted by 30 points per step and analysed in two szenarios: First, without pre-processing of the data by deseasonalization and second, with a deseasonalization before computing the drift slope. The analysis results are presented in figure 3. The results of the first approach are marked in blue with orange credibility bands defined as the 16 % to 84 % and 1 % to 99 % percentile of the drift slope posterior modelled by a kernel density estimate of the sampled parameters (Pedregosa et al. [2011]). The second ansatz is shown in red with the corresponding green credibility bands. Both estimation results can be compared to the analytical values of the smoothed partial derivative of the planktivore F -drift in planktivore F -direction shown as a black dotted line and computed with the data of the model realisations (cf. supplementary material (Heßler [2022])). The green dotted and orange solid vertical lines are defined equivalently to Perretti and Munch [2012] as the attractor switch point and the ‘‘point of no return’’, respectively, which is defined as the year in which even a reduction of the harvest rate to $qE = 0.1$ does not inhibit the destabilization process of the ecological system. The beginning of the grey shaded area is a subjectively defined time at which the previously small planktivore population exceeds 21 individuals and serves as an orientation for the ongoing destabilization process. Each column from left to right belongs to one of the three noise levels $\sigma = \{0.1, 2.2, 4.5\}$. The first (A-C), second (D-F) and third row (G-I) contain the drift slope results of the realisations of the model with additional white, pink and red noise, respectively. By comparing the results of the analyses with and without deseasonalization over various noise environments of the model we gain valuable insights into the capacities and limits of the methodological concept: In the figures 3 (A-C) the deseasonalized cases perform rather similar to the cases without deseasonalization apart from the weak noise case (A) with $\sigma = 0.1$. This leads to the conclusion that in the weak noise case (A) the seasonal effects in

the data are interpreted by the model probably in terms of noise fluctuations because the parameterization cannot capture the predominant seasonality. With increasing noise the seasonal effects become insignificant as visible in the figures 3 (B, C) because the noise level covers and hides the seasonal component of the data. The drift slope indicator seems to be suitable to provide information about the resilience of this ecological model with white noise, whereas seasonal aspects should be treated carefully for small noise levels. A comparison with the analytical partial derivative of the planktivore F -drift reveals that the deseasonalized estimates are accurate in the white noise cases. Technically, the drift slope estimation is not designed in order to deal with correlated noise and thus, with Non-Markovianity. As expected by that fact, the drift slope estimates in (D-I) exhibit a systematic quantitative estimation error compared to the analytical partial planktivore F -derivative. Nevertheless, the qualitative trends remain unchanged. Since the trend resolution towards a potentially zero-crossing is the crucial feature in terms of leading indicator use of the drift slope ζ the findings in (D-I) show that it can be still a helpful early warning tool even in highly correlated and noisy situations. Similar to the results in the weak white noise case (A) the results reach the critical zero line around the attractor switch point and exhibit less clear trends as their deseasonalized counterparts that reach the critical zero around the actual transition that is approximately marked by the beginning of the grey shaded area. In contrast to the white noise cases the seasonality in the correlated noise cases influences the results for all noise levels in a similar way: Without deseasonalization the drift slope reaches zero around the attractor switch point whereas it reaches zero around the point of no return in the absence of seasonality. The critical zero crossing of the drift slope in the deseasoned versions of the correlated noise cases seems to be a bit earlier than the crossings of the white noise counterparts. The high impact of the seasonality in the strong correlated noise cases compared to the strong white noise cases (B, C) is due to the correlation of the noise itself: The noise correlation tends to amplify or weaken the annual amplitudes, whereby the seasonal component of the time series is not hidden by the noise, but more or less preserved. Note also, that there is no clear formal reason for the zero crossing of the blue drift slopes at the attractor switch point or for the red drift slopes reaching the critical zero around the point of no return in the correlated noise cases. Besides, the strong fluctuating slope estimates after the transition time in figure 3 (D, G) without deseasonalization are numerical artefacts probably caused by the small correlated noise contributions in the new stable state.

In conclusion, the drift slope trends are rather robust in the presented model cases and provide reliable information about the resilience and destabilization of the ecological system. The method is relatively complicated to implement in contrast to leading indicator candidates as the AR1 or the std $\hat{\sigma}$. Anyhow, its performance and robustness could be important advantages in the field of ecology and other data-driven research as outlined in the next subsection 4.2 in which the performance of the drift slope in this dynamical rolling window setting is compared to common leading indicator candidates.

4.2 Comparison of leading indicators' performance

In order to compare the performance of the drift slope indicator with established early warning candidates as the autocorrelation at lag-1 (AR1), the standard deviation (std) $\hat{\sigma}$, the skewness γ or the kurtosis ω we use a Bayesian model comparison in which we compute the Bayes factors BF_{ij} with $i, j \in \{1, 2\}$ and $i \neq j$ that are defined as the ratio

$$BF_{ij} = \frac{p(\underline{\mathcal{I}}|\mathcal{M}_i)}{p(\underline{\mathcal{I}}|\mathcal{M}_j)} \quad (20)$$

of the evidences $p(\underline{\mathcal{I}}|\mathcal{M}_{1,2})$ that a linear trend model (model \mathcal{M}_1) or a constant model (model \mathcal{M}_2) explain the leading indicator datasets $\underline{\mathcal{I}}$ up to the ‘‘point of no return’’. The BF_{ij} are calculated for each of the above mentioned noise levels, noise types and the datasets without and with deseasonalization. A Bayes factor is declared to be significant for $BF_{ij} > 100$ (Jeffreys [1998]) to take into account the fact that most of the Bayes factors lie in the range $10 < BF_{ij} < 100$ or are significantly bigger than 100. The results of the comparison without deseasonalizing the data are summarized in table 2 where the color code follows Heßler and Kamps [2021] with a significant BF_{12} or BF_{21} marked by green and orange tiles, respectively, and grey tiles denote cases in which none of the models is favourable. The results of the kurtosis ω are excluded from further discussion, because of the ambiguous, non-monotone and very noisy trends with jumps which cannot be reliably interpreted by eye or captured by the linear model \mathcal{M}_1 of the Bayes model comparison. In some cases the constant model was erroneously preferred or the results were not significant. The corresponding curves of the leading indicators of each case can be found in the supplementary material (Heßler [2022]). Bayes factor pairs with infinite and zero entries correspond to one of the two models with evidence of zero and thus, the model with finite evidence is preferred. Without deseasonalization the common leading indicators AR1, std $\hat{\sigma}$ and skewness γ do not exhibit a significant slope following the Bayesian model comparison in most of the cases, although the time series resolution is relatively high (Perretti and Munch [2012]) and the time windows are chosen as big as in the last subsection 4.1. Without deseasonalization the AR1 just performs well in the white noise cases with $\sigma = \{2.2, 4.5\}$, whereas the skewness γ does not exhibit any reliable pattern of applicability. Note, that these results remain unchanged if the data is only detrended, but not deseasonalized. The corresponding analysis can be found in the supplementary material (Heßler [2022]). If the results are compared to the deseasonalized counterparts of table 3 the green tile of std $\hat{\sigma}$

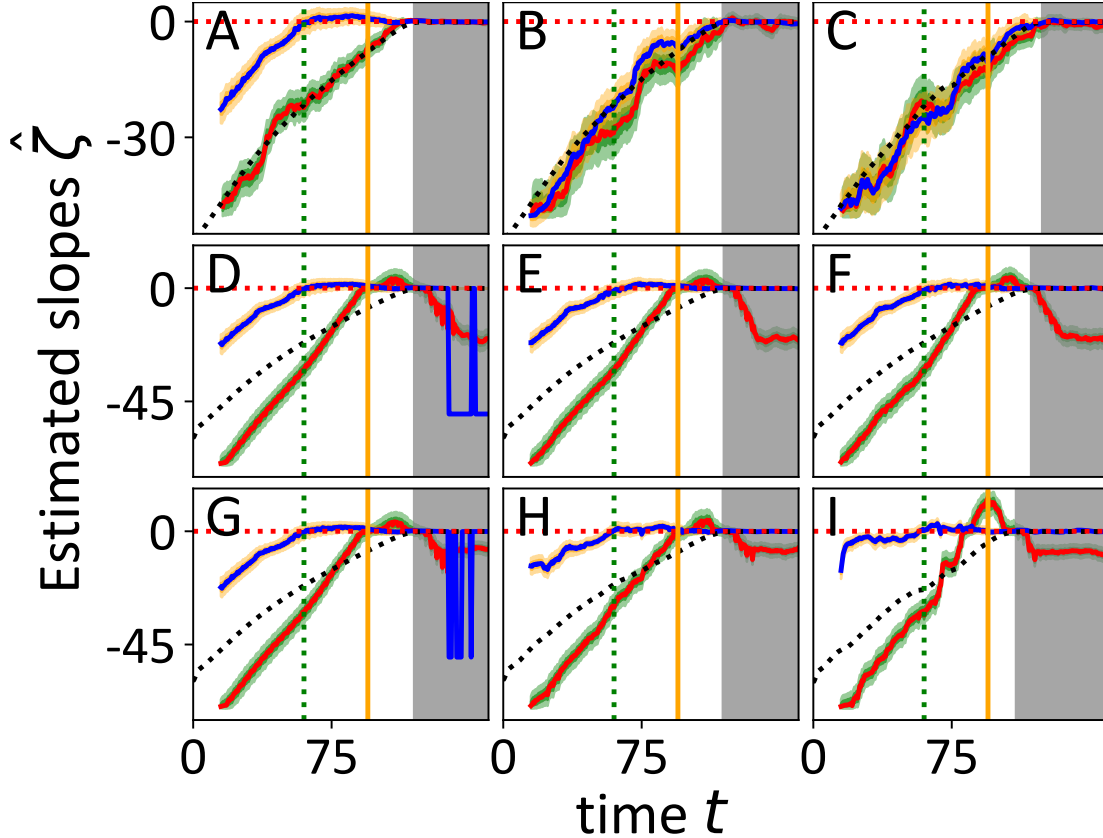


Figure 3: Results of the drift slope analysis for the ecological model with white (A-C), pink (D-F) and red noise (G-I). The columns from left to right correspond to the noise levels $\sigma = \{0.1, 2.2, 4.5\}$. The computations are performed on the time series without deseasonalization (blue lines with orange credibility bands) and with preparation by deseasonalizing the data (red lines with green credibility bands). The green dotted and the orange solid vertical lines indicate the attractor switch point of the deterministic system and the point of no return, respectively, that is defined as the time at which the destabilization cannot be stopped by reducing the harvest rate to $qE = 0.1$. A comparison of the drift slope estimates $\hat{\zeta}$ to the analytical partial planktivore F -drift slopes (black dotted lines) confirms that the estimates are quantitatively accurate in the case of white noise and qualitatively reasonable for correlated noise. The deseasonalized versions exhibit clear trends and reach the critical zero marked by the red dotted horizontal line around the transition time that is approximately signed by the beginning of the grey shaded area that is defined as the time at which the small planktivore population counts more than 21 individuals. Although, the method is not designed to deal with correlated noise and non-Markovian time series the seasonality of the data has much more influence than the correlated noise. The seasonality reduces clearness of the trends and leads to an earlier zero crossing of the drift slope for weak white and all correlated noise scenarios. In the weak white noise case the numerical method seems to interpret the seasonal effects incorrectly, probably as noise influence. For bigger noise levels the seasonal effects become insignificant for the white noise cases, but not for the correlated noise scenarios. The strong fluctuation of the drift slope estimates in the post transition region of the subfigures (D, G) are probably due to the small correlated noise contributions in the new stable state.

and the significant white noise cases of the skewness γ turn out to be artefacts caused by the seasonal nature of the time series. Interestingly, the deseasonalization leads to a consistent significance pattern of the skewness γ if only the correlated noise cases are considered. Therefore, the general applicability of the skewness γ as leading indicator is ill-advised since it is rather sensitive to noise types, seasonality and e.g. bistability of the system. Nevertheless, it could be useful under specific conditions as the correlated noise cases considered here or in flickering regimes of bistable systems. Only the recently proposed drift slope and the AR1 with deseasonalization seem to yield reliable results. The performance of the AR1 is significantly improved by deseasonalization that leads to significant trends in all cases as suggested by a comparison of the tables 3 and 2. Under the same conditions the drift slope turns out to be not very sensitive to the seasonal character of the data apart from the early plateaus discussed in subsection 4.1. The drift slope ζ leads to significant positive trends in all considered cases without distinction of non-deseasonalized and deseasonalized data. The results confirm in most instances the results of Perretti and Munch [2012] where a very poor applicability of the standard leading indicator candidates to the ecological test dataset is observed. The most robust leading indicator under strong noise was found to be the variance or std $\hat{\sigma}$ in Perretti and Munch [2012]. The Bayes factor analysis proposes AR1 to be the most reliable indicator of the standard measures and rejects the std $\hat{\sigma}$ as a robust indicator. Following the results of this study the drift slope ζ is a possible leading indicator candidate also in very noisy situations, provided that a suitable sampling rate of the time series is guaranteed. In the next subsection 4.3 the limitations of the drift slope estimates $\hat{\zeta}$ and their sensitivity to small window sizes are investigated because, as stated in Perretti and Munch [2012], ecological time series are often short and possible window sizes are strongly limited by that fact.

Table 2: Summary of the Bayes factors comparing a linear model \mathcal{M}_1 with positive slope to a constant model \mathcal{M}_2 for the drift slope ζ , the ARI, the std $\hat{\sigma}$ and the skewness γ for various noise types and levels without deseasonalization of the data. The kurtosis ω is excluded because of non-monotone behaviour. Green tiles mark a $BF_{12} > 100$ (Jeffreys [1998]) which is the threshold for a significant leading indicator trend. Grey tiles mark insignificant results. The constant model \mathcal{M}_2 is never preferred in the analysis. Infinite Bayes factors result from one model with evidence zero which leads to preferring the finite evidence model. Only the drift slope ζ performs well in the considered cases. The ARI has a very limited applicability and the skewness γ is not reliable over all cases. The green tile of the std $\hat{\sigma}$ is an artefact of the seasonality which is confirmed by a comparison with table 3. For completeness, the same analysis is performed for the skewness with a linear model \mathcal{M}_1 with negative slope in the supplementary material (Heßler [2022]).

noise level	white noise ($P_{\text{white}} \approx 7.5$)				pink noise ($P_{\text{pink}} \approx 2 \cdot P_{\text{white}}$)				red noise ($P_{\text{red}} \approx P_{\text{pink}}$)			
	$\sigma = 0.1$	$\sigma = 2.2$	$\sigma = 4.5$	$\sigma = 4.5$	$\sigma = 0.1$	$\sigma = 2.2$	$\sigma = 4.5$	$\sigma = 4.5$	$\sigma = 0.1$	$\sigma = 2.2$	$\sigma = 4.5$	$\sigma = 4.5$
indicator \underline{I}	BF ₁₂	BF ₁₂	BF ₁₂	BF ₁₂	BF ₁₂	BF ₁₂	BF ₁₂	BF ₁₂	BF ₁₂	BF ₁₂	BF ₁₂	BF ₁₂
	BF ₂₁	BF ₂₁	BF ₂₁	BF ₂₁	BF ₂₁	BF ₂₁	BF ₂₁	BF ₂₁	BF ₂₁	BF ₂₁	BF ₂₁	BF ₂₁
slope ζ	∞	∞	∞	∞	∞	∞	∞	∞	∞	∞	∞	$3.0 \cdot 10^{92}$
ARI	0	0	0	0	0	0	0	0	0	0	0	$3.3 \cdot 10^{-93}$
	12	$8.8 \cdot 10^7$	$3.8 \cdot 10^7$		9.4	8.7	9.1	9.5	3.1	3.1	3.1	1.2
std $\hat{\sigma}$	$8.3 \cdot 10^{-2}$	$1.1 \cdot 10^{-8}$	$2.6 \cdot 10^{-8}$		0.11	0.11	0.11	0.11	0.11	0.32	0.32	0.85
	19	18	57		18	18	39	19	10	10	10	$8.3 \cdot 10^4$
skewness γ	$5.3 \cdot 10^{-2}$	$5.5 \cdot 10^{-2}$	$1.8 \cdot 10^{-2}$		$5.5 \cdot 10^{-2}$	$5.5 \cdot 10^{-2}$	$2.6 \cdot 10^{-2}$	$5.4 \cdot 10^{-2}$	0.10	0.10	0.10	$1.2 \cdot 10^{-5}$
	$6.1 \cdot 10^6$	$1.3 \cdot 10^6$	0.91		$1.1 \cdot 10^7$	$9.5 \cdot 10^5$	$8.3 \cdot 10^8$	$1.1 \cdot 10^7$	61	61	61	$3.4 \cdot 10^4$
	$1.6 \cdot 10^{-7}$	$7.9 \cdot 10^{-7}$	1.1		$9.1 \cdot 10^{-8}$	$1.1 \cdot 10^{-6}$	$1.2 \cdot 10^{-9}$	$8.8 \cdot 10^{-8}$	$1.6 \cdot 10^{-2}$	$1.6 \cdot 10^{-2}$	$1.6 \cdot 10^{-2}$	$3.0 \cdot 10^{-5}$

Table 3: Same as table 2 with deseasonalization of the data. The drift slope ζ applies as before to all test cases. However, deseasonalization improves the performance of the ARI as leading indicator significantly as it also works for all deseasonalized cases, whereas the std $\hat{\sigma}$ does not work. This leads to the conclusion that the fragmentary applicability of the std $\hat{\sigma}$ in table 2 is an artefact due to a misinterpretation of the seasonal character of the time series. Confronted with these results it is important to keep in mind that the ARI is only a reliable indicator for a bifurcation-induced critical transition if the std increases at the same time. We could not find one case in which the Bayes factors of both ARI and std are decisive at the same time. The skewness becomes a reliable indicator for the considered correlated noise cases, whereas its positive trends disappear in the white noise cases due to the deseasonalization procedure. The same analysis for the skewness with a linear model \mathcal{M}_1 with negative slope can be found in the supplementary material (Heßler [2022]).

noise level	white noise ($P_{\text{white}} \approx 7.5$)			pink noise ($P_{\text{pink}} \approx 2 \cdot P_{\text{white}}$)			red noise ($P_{\text{red}} \approx P_{\text{pink}}$)		
	$\sigma = 0.1$	$\sigma = 2.2$	$\sigma = 4.5$	$\sigma = 0.1$	$\sigma = 2.2$	$\sigma = 4.5$	$\sigma = 0.1$	$\sigma = 2.2$	$\sigma = 4.5$
indicator \underline{I}	BF ₁₂	BF ₁₂	BF ₁₂	BF ₁₂	BF ₁₂	BF ₁₂	BF ₁₂	BF ₁₂	BF ₁₂
	BF ₂₁	BF ₂₁	BF ₂₁	BF ₂₁	BF ₂₁	BF ₂₁	BF ₂₁	BF ₂₁	BF ₂₁
slope ζ	∞	∞	∞	∞	∞	∞	∞	∞	∞
ARI	0	0	0	0	0	0	0	0	0
	$3.4 \cdot 10^5$	$1.6 \cdot 10^7$	$6.1 \cdot 10^6$	$4.3 \cdot 10^8$	$1.5 \cdot 10^8$	$1.4 \cdot 10^9$	$4.3 \cdot 10^8$	$1.4 \cdot 10^8$	$1.2 \cdot 10^9$
std $\hat{\sigma}$	$3.0 \cdot 10^{-6}$	$6.2 \cdot 10^{-8}$	$1.6 \cdot 10^{-7}$	$2.3 \cdot 10^{-9}$	$6.6 \cdot 10^{-9}$	$7.3 \cdot 10^{-10}$	$2.3 \cdot 10^{-9}$	$7.2 \cdot 10^{-9}$	$8.6 \cdot 10^{-10}$
	1.0	5.8	40	1.1	1.1	1.1	1.1	1.1	1.3
skewness γ	1.0	0.17	$2.5 \cdot 10^{-2}$	0.89	0.89	0.88	0.89	0.92	0.76
	14	0.58	0.44	$1.6 \cdot 10^{90}$	$3.6 \cdot 10^{89}$	$1.1 \cdot 10^{89}$	$1.8 \cdot 10^{90}$	$2.1 \cdot 10^{89}$	$2.3 \cdot 10^{93}$
	$7.1 \cdot 10^{-2}$	1.7	2.8	$6.3 \cdot 10^{-91}$	$2.8 \cdot 10^{-90}$	$8.8 \cdot 10^{-90}$	$5.7 \cdot 10^{-91}$	$4.7 \cdot 10^{-90}$	$4.4 \cdot 10^{-94}$

4.3 Window size limits

In order to ensure comparability of the results to Perretti and Munch [2012] the drift slope estimates are calculated for comparable window sizes and the corresponding $BF_{12,21}$ are calculated to get an impression of the minimal necessary amount of data per window that yields significant results. In Perretti and Munch [2012] a low-sampled time series variant with one measurement per year and a high-sampled variant of the time series with 50 data points per year is investigated. Here, we will focus on the high-sampled variants because the discussed indicators including the proposed drift slope are only applicable if the information level in terms of available data is high enough to resolve the considered dynamics. This remains a common limitation of the discussed indicators.

However, focusing on the high-sampled datasets with 50 points per year the $BF_{12,21}$ are calculated for window sizes $\{150, 100, 50, 25\}$ in decreasing order until the BF_{12} is no longer significant ($BF_{12} \leq 100$). The results for the discussed noise levels and types are summarized in table 4 without deseasonalization and in table 5 with deseasonalization. The color scheme is defined as in subsection 4.1. The tile is signed to be “inadequate” if both model evidences are numerically zero. A Bayes factor pair of infinite and zero indicates that one model has an evidence of zero and thus, does not fit the data at all. Without deseasonalization significant results are mainly generated for windows bigger than 50 and less or equal to 100 data points except for white noise with $\sigma = 0.1$ where windows less or equal to 50 data points are sufficient and pink noise with $\sigma = 4.5$ where windows have to be bigger than 100 data points. Thus, most of the significant windows include a time interval of one up to two years which is mostly comparable to the computations in Perretti and Munch [2012] assuming windows of one year. Furthermore, a suitable deseasonalization is able to decrease the necessary window size for significant drift slope trends even below one year between more than 25 and less or equal to 50 data points for pink and red noise. The performance for small windows tends to become slightly worse for the cases with small and strong white noise $\sigma = \{0.1, 4.5\}$. This is a sign for the difficulties of deseasonalization without removing valuable information for the drift slope estimation at the same time. It has to be mentioned that the drift slope trends for small window sizes as in this limit cases are volatile and thus, less appropriate for an on-line analysis approach.

Table 4: Summary of the Bayes factors comparing a linear model \mathcal{M}_1 to a constant model \mathcal{M}_2 for the small window sizes of $\{150, 100, 50\}$ for various noise types and levels without deseasonalization of the data. Model \mathcal{M}_1 is preferred upon the threshold $BF_{12} > 100$ (Jeffreys [1998]) colored in green. Grey tiles are insignificant results. The constant model \mathcal{M}_2 is never preferred. If both models had an evidence that resulted in a numerical zero, the tile is marked as “inadequate”, because none of the models was adequate to fit the data. In the case that one evidence was finite and one zero the Bayes factor ratio becomes infinite indicating that the model with an evidence of zero does not fit the data at all and thus, the other one is preferred. The results tend to be significant for more than 50 and less than or equal to 100 data points per window except for the red noise with $\sigma = 4.5$ that becomes significant for more than 100 and less than or equal to 150 data points. The white noise case with $\sigma = 0.1$ is already significant for less than or equal to 50 data points. The infinite BF_{12} of the pink noise system with noise level $\sigma = 4.5$ is written in brackets and colored in grey, because the trend is very noisy. This corresponds to a period in time between one and two years of high-sampled observation of the ecological system.

noise level	white noise ($P_{\text{white}} \approx 7.5$)			pink noise ($P_{\text{pink}} \approx 2 \cdot P_{\text{white}}$)			red noise ($P_{\text{red}} \approx P_{\text{pink}}$)		
	$\sigma = 0.1$	$\sigma = 2.2$	$\sigma = 4.5$	$\sigma = 0.1$	$\sigma = 2.2$	$\sigma = 4.5$	$\sigma = 0.1$	$\sigma = 2.2$	$\sigma = 4.5$
window size	BF_{12} BF_{21}	BF_{12} BF_{21}	BF_{12} BF_{21}	BF_{12} BF_{21}	BF_{12} BF_{21}	BF_{12} BF_{21}	BF_{12} BF_{21}	BF_{12} BF_{21}	BF_{12} BF_{21}
50	$2.6 \cdot 10^5$ $3.9 \cdot 10^{-6}$	inadequate inadequate	inadequate	$1.6 \cdot 10^{-2}$ 63	$1.2 \cdot 10^{-2}$ 84	(∞) (0)	79 $1.3 \cdot 10^{-2}$	1.2 0.85	inadequate
100	∞ 0	∞ 0	∞ 0	∞ 0	∞ 0	∞ 0	∞ 0	∞ 0	inadequate
150	∞ 0	∞ 0	∞ 0	∞ 0	∞ 0	∞ 0	∞ 0	∞ 0	∞ 0

Table 5: Same as table 4 for window sizes of $\{150, 100, 50, 25\}$ with deseasonalization of the data. A deseasonalization decreases the necessary data per window to generate significant results to less than or equal to 50 and more than 25 data points for all pink and red noise cases. This corresponds to time periods of a half year up to one year of observation in a high-sampled manner. The slightly worse results for the white noise cases give a hint that the method reacts sensitive to the deseasonalization in that noise case.

noise level	white noise ($P_{\text{white}} \approx 7.5$)				pink noise ($P_{\text{pink}} \approx 2 \cdot P_{\text{white}}$)				red noise ($P_{\text{red}} \approx P_{\text{pink}}$)			
	$\sigma = 0.1$	$\sigma = 2.2$	$\sigma = 4.5$	$\sigma = 7.5$	$\sigma = 0.1$	$\sigma = 2.2$	$\sigma = 4.5$	$\sigma = 7.5$	$\sigma = 0.1$	$\sigma = 2.2$	$\sigma = 4.5$	$\sigma = 7.5$
window size	BF ₁₂	BF ₁₂	BF ₁₂	BF ₁₂	BF ₁₂	BF ₁₂	BF ₁₂	BF ₁₂	BF ₁₂	BF ₁₂	BF ₁₂	BF ₁₂
	BF ₂₁	BF ₂₁	BF ₂₁	BF ₂₁	BF ₂₁	BF ₂₁	BF ₂₁	BF ₂₁	BF ₂₁	BF ₂₁	BF ₂₁	BF ₂₁
25	-	-	-	-	inadequate	inadequate	inadequate	inadequate	inadequate	inadequate	inadequate	inadequate
50	inadequate	inadequate	inadequate	inadequate	∞	∞	∞	∞	∞	∞	∞	∞
	∞	∞	∞	∞	0	0	0	0	0	0	0	0
100	∞	∞	inadequate	inadequate	∞	∞	∞	∞	∞	∞	∞	∞
	0	0	0	0	0	0	0	0	0	0	0	0
150	∞	∞	∞	∞	∞	∞	∞	∞	∞	∞	∞	∞
	0	0	0	0	0	0	0	0	0	0	0	0

5 Summary and conclusion

Our investigations are based on the destabilizing ecological model previously considered in Perretti and Munch [2012] with white, correlated and weak up to strong noise geared to real world experimental data. The simulations are almost comparable except for a slightly longer period of data sampling before the “point of no return”.

The main difficulties stated in Perretti and Munch [2012] concerning the applicability of established leading indicator candidates as AR1, std $\hat{\sigma}$, skewness γ and kurtosis ω are given by the conditions of ecological data acquisition: Normally, just short time series with a low sampling rate and strong noise are available. Furthermore, the systems tend to be influenced by correlated pink or red noise and seasonality. The above mentioned early warning signals fail under these circumstances especially due to low data availability for their estimation and high noise levels. Besides, even under favourable simulation conditions the leading indicator candidates are not as reliable as necessary for management decisions (Biggs et al. [2009]). In the course of this work we have introduced an alternative leading indicator, the so-called “drift slope”, and evaluated its performance in comparison to the common leading indicators mentioned above. The drift slope is derived from the MCMC-estimated parameters of the drift term of a stochastic differential equation while the drift term is approximated by a third-order Taylor polynomial.

We could show that the drift slope gives reliable trends to estimate the resilience of the system almost regardless of the noise level and type and it fulfills the demands for an early warning signal stated by Biggs et al. [2009] which we cite in section 1: The drift slope

- (i) exhibits a clear threshold of destabilization at zero and the relative distance to zero measures the level of resilience,
- (ii) provides trends which are easy-to-interpret regarding the necessity of management action,
- (iii) is comparable across systems in similar contexts because of its parametric ansatz and quantitative nature.

The standard measures skewness γ and kurtosis ω turn out to usually fail to predict the destabilization process which coincides with the observations in Perretti and Munch [2012]. The kurtosis ω exhibits non-monotone or ambiguous behaviour and is not suited to be applied as leading indicator in this study. Without deseasonalization the skewness γ shows only fragmentary significant results and thus, is not reliable over the range of the considered cases. With deseasonalization the skewness γ yields at least significant results under correlated noise conditions. In contrast to the results of Perretti and Munch [2012] the std $\hat{\sigma}$ also fails to generate significant results whereas the AR1 seems to be the most robust of the standard measures. Nevertheless, the AR1 is very sensitive to the seasonality of the time series that seems to play an important role in the calculations of the leading indicators in general. Deseasonalization has to be taken into account to achieve optimal results, if the noise intensity does not hide the seasonal component. Accordingly, the applicability of the AR1 is enlarged to correlated situations and the clearness of the drift slope trends could be improved. Furthermore, the minimum of necessary data per window for the drift slope estimation could be diminished due to a deseasonalization of the time series. The minimum of available data for the pink and red noise cases is decreased from between 50 and 100 to 25 – 50 data points except for the red noise case with $\sigma = 4.5$ and thus lie in the observation range of one year or less. The white noise cases do not benefit in that way from a deseasonalization. We considered the destabilization due to a bifurcation, but in principle the Langevin estimation lends itself to monitor changes of the noise level at the same time which can be crucial for systems with the threat of noise-induced transitions (cf. figure 5 (Heßler and Kamps [2021])).

In the end, the drift slope could be an interesting alternative in order to deal with very noisy correlated data under typical circumstances in ecology and other fields, but it is limited due to the available amount of data. The low-sampled scenarios with one point per year are impossible to handle neither with the drift slope estimation nor with the standard measures. However, in some cases the opportunities of tracking resilience with the drift slope measure might be an attractive reason to improve sampling-rates and data collection e.g. by using deep-learning image recognition techniques (Francisco et al. [2020], Duporge et al. [2020], Zhao et al. [2020], Aspillaga et al. [2021]) for experimental and management purposes, wherever possible.

Data and software availability

The simulated data and Python codes are available on github via https://github.com/MartinHessler/Quantifying_resilience_under_realistic_noise under a *GNU General Public License v3.0*. The open source python-implementation of the described methods is named *antiCPy* and can be found at <https://github.com/MartinHessler/antiCPy> under a *GNU General Public License v3.0*.

Acknowledgements

M. H. thanks the Studienstiftung des deutschen Volkes for a scholarship including financial support. We thank colleagues and friends for proofreading the manuscript.

References

- Vasilis Dakos, Stephen R. Carpenter, William A. Brock, Aaron M. Ellison, Vishwesh Guttal, Anthony R. Ives, Sonia Kéfi, Valerie Livina, David A. Seekell, Egbert H. van Nes, and Marten Scheffer. Methods for detecting early warnings of critical transitions in time series illustrated using simulated ecological data. *PLoS ONE*, 7(7):e41010, jul 2012. doi:10.1371/journal.pone.0041010.
- Vasilis Dakos, Egbert H. van Nes, Raúl Donangelo, Hugo Fort, and Marten Scheffer. Spatial correlation as leading indicator of catastrophic shifts. *Theoretical Ecology*, 3(3):163–174, nov 2009. doi:10.1007/s12080-009-0060-6.
- Marten Scheffer, Stephen R. Carpenter, Vasilis Dakos, and Egbert H. van Nes. Generic indicators of ecological resilience: Inferring the chance of a critical transition. *Annual Review of Ecology, Evolution, and Systematics*, 46(1): 145–167, dec 2015. doi:10.1146/annurev-ecolsys-112414-054242.
- Junhao Liang, Yanqing Hu, Guanrong Chen, and Tianshou Zhou. A universal indicator of critical state transitions in noisy complex networked systems. *Scientific Reports*, 7(1), feb 2017. doi:10.1038/srep42857.
- Annelies J. Veraart, Elisabeth J. Faassen, Vasilis Dakos, Egbert H. van Nes, Miquel Lurling, and Marten Scheffer. Recovery rates reflect distance to a tipping point in a living system. *Nature*, 481(7381):357–359, dec 2011. doi:10.1038/nature10723.
- John M. Drake and Blaine D. Griffen. Early warning signals of extinction in deteriorating environments. *Nature*, 467(7314):456–459, sep 2010. doi:10.1038/nature09389.
- Vasilis Dakos, Sarah M. Glaser, Chih hao Hsieh, and George Sugihara. Elevated nonlinearity as an indicator of shifts in the dynamics of populations under stress. *Journal of The Royal Society Interface*, 14(128):20160845, mar 2017. doi:10.1098/rsif.2016.0845.
- V. N. Livina, F. Kwasiok, and T. M. Lenton. Potential analysis reveals changing number of climate states during the last 60 kyr. *Climate of the Past*, 6(1):77–82, feb 2010. doi:10.5194/cp-6-77-2010.
- V. N. Livina, T. M. Vaz Martins, and A. B. Forbes. Tipping point analysis of atmospheric oxygen concentration. *Chaos: An Interdisciplinary Journal of Nonlinear Science*, 25(3):036403, mar 2015. doi:10.1063/1.4907185.
- Timothy M. Lenton. Arctic climate tipping points. *AMBIO*, 41(1):10–22, jan 2012. doi:10.1007/s13280-011-0221-x.
- Eduardo Cotilla-Sanchez, Paul D. H. Hines, and Christopher M. Danforth. Predicting critical transitions from time series synchrophasor data. *IEEE Transactions on Smart Grid*, 3(4):1832–1840, dec 2012. doi:10.1109/tsg.2012.2213848.
- Marko Jusup, Petter Holme, Kiyoshi Kanazawa, Misako Takayasu, Ivan Romić, Zhen Wang, Sunčana Geček, Tomislav Lipić, Boris Podobnik, Lin Wang, Wei Luo, Tin Klanjšček, Jingfang Fan, Stefano Boccaletti, and Matjaž Perc. Social physics. *Physics Reports*, 948:1–148, feb 2022. doi:10.1016/j.physrep.2021.10.005.
- Dirk Helbing, Dirk Brockmann, Thomas Chadeaux, Karsten Donnay, Ulf Blanke, Olivia Woolley-Meza, Mehdi Moussaid, Anders Johansson, Jens Krause, Sebastian Schutte, and Matjaž Perc. Saving human lives: What complexity science and information systems can contribute. *Journal of Statistical Physics*, 158(3):735–781, jun 2014. doi:10.1007/s10955-014-1024-9.
- Igor Izrailtyan, J. Yasha Kresh, Rohinton J. Morris, Susan C. Brozena, Steven P. Kutalek, and Andrew S. Wechsler. Early detection of acute allograft rejection by linear and nonlinear analysis of heart rate variability. *The Journal of Thoracic and Cardiovascular Surgery*, 120(4):737–745, 2000. ISSN 0022-5223. doi:https://doi.org/10.1067/mtc.2000.108930. URL <http://www.sciencedirect.com/science/article/pii/S0022522300329877>.
- Thomas Chadeaux. Early warning signals for war in the news. *Journal of Peace Research*, 51(1):5–18, jan 2014. doi:10.1177/0022343313507302.
- I. A. van de Leemput, M. Wichers, A. O. J. Cramer, D. Borsboom, F. Tuerlinckx, P. Kuppens, E. H. van Nes, W. Viechtbauer, E. J. Giltay, S. H. Aggen, C. Derom, N. Jacobs, K. S. Kendler, H. L. J. van der Maas, M. C. Neale, F. Peeters, E. Thiery, P. Zachar, and M. Scheffer. Critical slowing down as early warning for the onset and termination of depression. *Proceedings of the National Academy of Sciences*, 111(1):87–92, dec 2013. doi:10.1073/pnas.1312114110.
- Christopher F. Clements, John M. Drake, Jason I. Griffiths, and Arpat Ozgul. Factors influencing the detectability of early warning signals of population collapse. *The American Naturalist*, 186(1):50–58, jul 2015. doi:10.1086/681573.
- Alan Hastings and Derin B. Wysham. Regime shifts in ecological systems can occur with no warning. *Ecology Letters*, 13(4):464–472, apr 2010. doi:10.1111/j.1461-0248.2010.01439.x.

- Peter D. Ditlevsen and Sigfus J. Johnsen. Tipping points: Early warning and wishful thinking. *Geophysical Research Letters*, 37(19):n/a–n/a, oct 2010. doi:10.1029/2010gl044486.
- Theresa Wilkat, Thorsten Rings, and Klaus Lehnertz. No evidence for critical slowing down prior to human epileptic seizures. *Chaos: An Interdisciplinary Journal of Nonlinear Science*, 29(9):091104, sep 2019. doi:10.1063/1.5122759.
- Marten Scheffer, Jordi Bascompte, William A. Brock, Victor Brovkin, Stephen R. Carpenter, Vasilis Dakos, Hermann Held, Egbert H. van Nes, Max Rietkerk, and George Sugihara. Early-warning signals for critical transitions. *Nature*, 461(7260):53–59, sep 2009. doi:10.1038/nature08227.
- Paul Ritchie and Jan Sieber. Probability of noise- and rate-induced tipping. *Physical Review E*, 95(5), may 2017. doi:10.1103/physreve.95.052209.
- Peter Ashwin, Sebastian Wieczorek, Renato Vitolo, and Peter Cox. Tipping points in open systems: bifurcation, noise-induced and rate-dependent examples in the climate system. *Philosophical Transactions of the Royal Society A: Mathematical, Physical and Engineering Sciences*, 370(1962):1166–1184, mar 2012. doi:10.1098/rsta.2011.0306.
- Marten Scheffer, Stephen R. Carpenter, Timothy M. Lenton, Jordi Bascompte, William Brock, Vasilis Dakos, Johan van de Koppel, Ingrid A. van de Leemput, Simon A. Levin, Egbert H. van Nes, Mercedes Pascual, and John Vandermeer. Anticipating critical transitions. *Science*, 338(6105):344–348, 2012. ISSN 0036-8075. doi:10.1126/science.1225244. URL <http://science.sciencemag.org/content/338/6105/344>.
- C. Wissel. A universal law of the characteristic return time near thresholds. *Oecologia*, 65(1):101–107, dec 1984. doi:10.1007/bf00384470.
- Arne Schröder, Lennart Persson, André M. de Roos, and Per Lundberg. Direct experimental evidence for alternative stable states: A review. *Oikos*, 110(1):3–19, 2005. ISSN 00301299, 16000706. URL <http://www.jstor.org/stable/3548414>.
- Maarten C. Boerlijst, Thomas Oudman, and André M. de Roos. Catastrophic collapse can occur without early warning: Examples of silent catastrophes in structured ecological models. *PLoS ONE*, 8(4):e62033, apr 2013. doi:10.1371/journal.pone.0062033.
- Carl Boettiger and Alan Hastings. Early warning signals and the prosecutor's fallacy. *Proceedings of the Royal Society B: Biological Sciences*, 279(1748):4734–4739, oct 2012. doi:10.1098/rspb.2012.2085.
- Charles T. Perretti and Stephan B. Munch. Regime shift indicators fail under noise levels commonly observed in ecological systems. *Ecological Applications*, 22(6):1772–1779, sep 2012. doi:10.1890/11-0161.1.
- Alena Sonia Gsell, Ulrike Scharfenberger, Deniz Özkundakci, Annika Walters, Lars-Anders Hansson, Annette B. G. Janssen, Peeter Nõges, Philip C. Reid, Daniel E. Schindler, Ellen Van Donk, Vasilis Dakos, and Rita Adrian. Evaluating early-warning indicators of critical transitions in natural aquatic ecosystems. *Proceedings of the National Academy of Sciences*, 113(50):E8089–E8095, nov 2016. doi:10.1073/pnas.1608242113.
- Fabian Dablander, Anton Pichler, Arta Cika, and Andrea Bacilieri. Anticipating critical transitions in psychological systems using early warning signals: Theoretical and practical considerations. *PsyArXiv*, oct 2020. doi:10.31234/osf.io/5wc28.
- John A. Bissonette. Small sample size problems in wildlife ecology: a contingent analytical approach. *Wildlife Biology*, 5(2):65–71, 1999. doi:https://doi.org/10.2981/wlb.1999.010. URL <https://onlinelibrary.wiley.com/doi/abs/10.2981/wlb.1999.010>.
- Fritz A Francisco, Paul Nührenberg, and Alex Jordan. High-resolution, non-invasive animal tracking and reconstruction of local environment in aquatic ecosystems. *Movement Ecology*, 8(1), jun 2020. doi:10.1186/s40462-020-00214-w.
- Isla Duporge, Olga Isupova, Steven Reece, David W. Macdonald, and Tiejun Wang. Using very-high-resolution satellite imagery and deep learning to detect and count african elephants in heterogeneous landscapes. *Remote Sensing in Ecology and Conservation*, 7(3):369–381, dec 2020. doi:10.1002/rse2.195.
- Peng Zhao, Shuming Liu, Yi Zhou, Tim Lynch, Wenhui Lu, Tao Zhang, and Hongsheng Yang. Estimating animal population size with very high-resolution satellite imagery. *Conservation Biology*, 35(1):316–324, nov 2020. doi:10.1111/cobi.13613.
- Eneko Aspillaga, Robert Arlinghaus, Martina Martorell-Barceló, Guillermo Follana-Berná, Arancha Lana, Andrea Campos-Candela, and Josep Alós. Performance of a novel system for high-resolution tracking of marine fish societies. *Animal Biotelemetry*, 9(1), jan 2021. doi:10.1186/s40317-020-00224-w.
- Reinette Biggs, Stephen R. Carpenter, and William A. Brock. Turning back from the brink: Detecting an impending regime shift in time to avert it. *Proceedings of the National Academy of Sciences*, 106(3):826–831, jan 2009. doi:10.1073/pnas.0811729106.

- Martin Heßler and Oliver Kamps. Bayesian on-line anticipation of critical transitions. *New Journal of Physics*, dec 2021. doi:10.1088/1367-2630/ac46d4.
- Martin Heßler. antiCPy. <https://github.com/MartinHessler/antiCPy>, 2021a. URL <https://github.com/MartinHessler/antiCPy>.
- Martin Heßler. antiCPy’s documentation. <https://anticpy.readthedocs.io>, 2021b. URL <https://anticpy.readthedocs.io>.
- S. R. Carpenter and W. A. Brock. Early warnings of unknown nonlinear shifts: a nonparametric approach. *Ecology*, 92(12):2196–2201, dec 2011. doi:10.1890/11-0716.1.
- Peter E. Kloeden and Eckhard Platen. *Numerical Solution of Stochastic Differential Equations*. Springer Berlin Heidelberg, 1992. doi:10.1007/978-3-662-12616-5.
- R. Friedrich and J. Peinke. Description of a turbulent cascade by a fokker-planck equation. *Phys. Rev. Lett.*, 78:863–866, Feb 1997. doi:10.1103/PhysRevLett.78.863. URL <https://link.aps.org/doi/10.1103/PhysRevLett.78.863>.
- R. Friedrich, S. Siegert, J. Peinke, St. Lück, M. Siefert, M. Lindemann, J. Raethjen, G. Deuschl, and G. Pfister. Extracting model equations from experimental data. *Physics Letters A*, 271(3):217–222, jun 2000. doi:10.1016/s0375-9601(00)00334-0.
- Martin Heßler. Supplementary information. https://github.com/MartinHessler/Quantifying_resilience_under_realistic_noise, October 2022. URL https://github.com/MartinHessler/Quantifying_resilience_under_realistic_noise.
- David Kleinhans. Estimation of drift and diffusion functions from time series data: A maximum likelihood framework. *Physical review. E, Statistical, nonlinear, and soft matter physics*, 85, 10 2011. doi:10.1103/PhysRevE.85.026705.
- S. R. Carpenter and W. A. Brock. Spatial complexity, resilience and policy diversity: fishing on lake-rich landscapes. *Ecology and Society*, 9(1):8, 2004. URL <http://www.ecologyandsociety.org/vol9/iss1/art8>.
- David H. Reed and Gayla R. Hobbs. The relationship between population size and temporal variability in population size. *Animal Conservation*, 7(1):1–8, feb 2004. doi:10.1017/s1367943004003476.
- John H. Steele. A comparison of terrestrial and marine ecological systems. *Nature*, 313(6001):355–358, jan 1985. doi:10.1038/313355a0.
- David A. Vasseur and Peter Yodzis. THE COLOR OF ENVIRONMENTAL NOISE. *Ecology*, 85(4):1146–1152, apr 2004. doi:10.1890/02-3122.
- J Pope. An evaluation of the stock structure of north sea cod, haddock, and whiting since 1920, together with a consideration of the impacts of fisheries and predation effects on their biomass and recruitment. *ICES Journal of Marine Science*, 53(6):1157–1169, dec 1996. doi:10.1006/jmsc.1996.0141.
- Steven H. Strogatz. *Nonlinear dynamics and chaos. With Applications to Physics, Biology, Chemistry and Engineering*. Westview Press, second edition edition, 2015.
- Wolfgang von der Linden, Volker Dose, and Udo von Tussaint. *Bayesian Probability Theory. Applications in the Physical Sciences*. Cambridge University Press, 2014.
- Daniel Foreman-Mackey, David W. Hogg, Dustin Lang, and Jonathan Goodman. emcee: The MCMC hammer. *Publications of the Astronomical Society of the Pacific*, 125(925):306–312, mar 2013. doi:10.1086/670067.
- Skipper Seabold and Josef Perktold. statsmodels: Econometric and statistical modeling with python. In *9th Python in Science Conference*, 2010.
- Charles R. Harris, K. Jarrod Millman, Stéfan J. van der Walt, Ralf Gommers, Pauli Virtanen, David Cournapeau, Eric Wieser, Julian Taylor, Sebastian Berg, Nathaniel J. Smith, Robert Kern, Matti Picus, Stephan Hoyer, Marten H. van Kerkwijk, Matthew Brett, Allan Haldane, Jaime Fernández del Río, Mark Wiebe, Pearu Peterson, Pierre Gérard-Marchant, Kevin Sheppard, Tyler Reddy, Warren Weckesser, Hameer Abbasi, Christoph Gohlke, and Travis E. Oliphant. Array programming with NumPy. *Nature*, 585(7825):357–362, sep 2020. doi:10.1038/s41586-020-2649-2.
- Pauli Virtanen, Ralf Gommers, Travis E. Oliphant, Matt Haberland, Tyler Reddy, David Cournapeau, Evgeni Burovski, Pearu Peterson, Warren Weckesser, Jonathan Bright, Stéfan J. van der Walt, Matthew Brett, Joshua Wilson, K. Jarrod Millman, Nikolay Mayorov, Andrew R. J. Nelson, Eric Jones, Robert Kern, Eric Larson, C J Carey, İlhan Polat, Yu Feng, Eric W. Moore, Jake VanderPlas, Denis Laxalde, Josef Perktold, Robert Cimrman, Ian Henriksen, E. A. Quintero, Charles R. Harris, Anne M. Archibald, Antônio H. Ribeiro, Fabian Pedregosa, Paul van Mulbregt, and SciPy 1.0 Contributors. SciPy 1.0: Fundamental Algorithms for Scientific Computing in Python. *Nature Methods*, 17:261–272, 2020. doi:10.1038/s41592-019-0686-2.

Harold Jeffreys. *Theory of Probability*. OUP Oxford, August 1998. ISBN 0198503687. URL https://www.ebook.de/de/product/3605842/harold_jeffreys_theory_of_probability.html.

Fabian Pedregosa, Gaël Varoquaux, Alexandre Gramfort, Vincent Michel, Bertrand Thirion, Olivier Grisel, Mathieu Blondel, Peter Prettenhofer, Ron Weiss, Vincent Dubourg, Jake Vanderplas, Alexandre Passos, David Cournapeau, Matthieu Brucher, Matthieu Perrot, and Édouard Duchesnay. Scikit-learn: Machine learning in python. *Journal of Machine Learning Research*, 12(85):2825–2830, 2011. URL <http://jmlr.org/papers/v12/pedregosa11a.html>.